Journal of Biomechanics 49 (2016) 1437–1446

Contents lists available at ScienceDirect

Journal of Biomechanics

journal homepage: www.elsevier.com/locate/jbiomech
www.JBiomech.com

Analysis of non-Newtonian effects on Low-Density Lipoprotein accumulation in an artery

Marcello Iasiello [a,b], Kambiz Vafai [a,*], Assunta Andreozzi [b], Nicola Bianco [b]

[a] Department of Mechanical Engineering, University of California, Riverside, CA 92521, USA
[b] Dipartimento di Ingegneria Industriale, Università degli Studi di Napoli Federico II, P.le Tecchio, 80, Napoli 80125, Italy

ARTICLE INFO

Article history:
Accepted 10 March 2016

Keywords:
Non-Newtonian effects
LDL transport
Rheological models
Aorta–common iliac bifurcation

ABSTRACT

In this work, non-Newtonian effects on Low-Density Lipoprotein (LDL) transport across an artery are analyzed with a multi-layer model. Four rheological models (Carreau, Carreau–Yasuda, power-law and Newtonian) are used for the blood flow through the lumen. For the non-Newtonian cases, the arterial wall is modeled with a generalized momentum equation. Convection–diffusion equation is used for the LDL transport through the lumen, while Staverman–Kedem–Katchalsky, combined with porous media equations, are used for the LDL transport through the wall. Results are presented in terms of filtration velocity, Wall Shear Stresses (WSS) and concentration profiles. It is shown that non-Newtonian effects on mass transport are negligible for a healthy intramural pressure value. Non-Newtonian effects increase slightly with intramural pressure, but Newtonian assumption can still be considered reliable. Effects of arterial size are also analyzed, showing that Newtonian assumption can be considered valid for both medium and large arteries, in predicting LDL deposition. Finally, non-Newtonian effects are also analyzed for an aorta–common iliac bifurcation, showing that Newtonian assumption is valid for mass transport at low Reynolds numbers. At a high Reynolds number, it has been shown that a non-Newtonian fluid model can have more impact due to the presence of flow recirculation.

1. Introduction

While the mechanisms of plaque formation are still not fully understood (Keller et al., 2011), it is widely known that Low-Density Lipoprotein (LDL) has a primary role in its formation. Plaque formation is considered to be the cause of cardiovascular diseases, which currently is the first cause of death in the world (Taylor et al., 2013). For this reason, an exhaustive description of LDL deposition through an arterial wall is very important.

A multi-layer wall model is the most accurate way to predict mass transport through an arterial wall (Yang and Vafai, 2006; Ai and Vafai, 2006). This is because it takes into account the heterogeneity of an arterial wall, predicting LDL accumulation more accurately than a wall-free or a single-layer model. An arterial wall can be modeled by using the porous membrane Staverman–Kedem–Katchalsky equations, coupled with a reaction term for the tunica media. Closing coefficients based on pore theory or fiber matrix models have been developed during the years (Huang et al., 1997; Tada and Tarbell, 2000; Ai and Vafai, 2006; Chung and Vafai, 2012). Many studies were carried out during the years to analyze physical phenomena that are of relevance in the LDL deposition through an artery (Fazli et al., 2011; Lantz and Karlsson, 2012; Nematollahi et al., 2015). Pulsatile flow and osmosis effects were analyzed by Yang and Vafai (2006), while stenosis effects were depicted for an isothermal artery by Ai and Vafai (2006), Chung and Vafai (2013), and with a hyperthermia load, by Iasiello et al. (2015). Fluid–structure interactions were analyzed by Chung and Vafai (2012), Sun et al. (2015) and Vallez et al. (2015), and later under hyperthermia loads (Chung and Vafai, 2014). Realistic arteries studies were also carried out by Kenjereš and de Loor (2014). Furthermore, pertinent analytical solutions were obtained establishing the details of LDL transport within an artery (Yang and Vafai, 2008; Khakpour and Vafai, 2008a; Wang and Vafai, 2013, 2015). The aforementioned studies have utilized the Newtonian model for the blood flow.

In general the blood can act as a non-Newtonian fluid (Ross Ethier and Simmons, 2007). However, many studies have argued that for large arteries (Cho and Kensey, 1991; Lou and Yang, 1993; Perktold et al., 1999; Johnston et al., 2004; Mandal, 2005; Johnston et al., 2006; Ross Ethier and Simmons, 2007; Yilmaz and Gundogdu, 2008), and in some cases for medium arteries (Ross Ethier and Simmons, 2007), the blood flow can be considered to be Newtonian. Several studies have discussed the influence of non-Newtonian characteristics on the blood flow. Johnston et al. (2004)

* Corresponding author.
E-mail address: vafai@engr.ucr.edu (K. Vafai).

http://dx.doi.org/10.1016/j.jbiomech.2016.03.017
0021-9290/

Nomenclature

Latin letters

c	LDL concentration (mol/m^3)
C	form coefficient (1/m)
d	diameter (m)
D	LDL mass diffusivity (m^2/s)
$\vec{g}$	gravitational acceleration (m/s^2)
k	first-order reaction coefficient (1/s)
K	hydraulic permeability (m^2)
K^*	power-law fluid permeability (m^2)
n	power-law index
p	hydraulic pressure (Pa)
q	Carreau–Yasuda fluid coefficient
r	radius (m)
Re	Reynolds number
u, v	velocity components (m/s)
$\vec{V}$	velocity vector (m/s)
WSS	Wall Shear Stresses (Pa)
z	axial coordinate (m)

Greek letters

$\dot{\gamma}$	shear rate (1/s)
ε	porosity
μ	dynamic viscosity (mPa s)
μ^*	fluid consistency (mPa s^n)
λ	relaxation time (s)
ρ	density (kg/m^3)
σ	Staverman reflection coefficient
$\overline{\overline{\tau}}$	stress tensor
χ	tortuosity factor

Subscripts

0	reference
eff	effective property
lumen	lumen
m	mean
z	zero shear rate
∞	infinite shear rate

defined an index that quantifies the importance of non-Newtonian effects for both steady state and transient state (Johnston et al., 2006). This index has been extended on stenosed arteries by Razavi et al. (2011), who have also stated that Carreau and Carreau–Yasuda are the two models that provide closer results to a Newtonian model. Ross Either and Simmons (2007) have reported some typical hemodynamic values for a 70 kg human. They had concluded that, for the typical shear rate values, blood can be treated as Newtonian for most of the large arteries. Newtonian assumption can incur some inaccuracy, for example when hematocrit level is increasing (Yilmaz and Gundogdu, 2008; Mandal, 2005), or when Wall Shear Stresses (WSS) become lower (bends, bifurcations, fluid separation or recirculation zone) (Cho and Kensey, 1991; Lou and Yang, 1993; Mandal, 2005). For the non-Newtonian effects on LDL transport, there are few studies, such as Liu et al. (2011), who have investigated non-Newtonian effects on LDL through the human aorta by using a wall free model constructed from MRI images. They found that non-Newtonian effects are relatively insignificant on the LDL concentration in most regions of the aorta. However, non-Newtonian effects become pronounced in areas with flow disturbance, for both steady state and pulsatile flow cases. Hong et al. (2012) analyzed the non-Newtonian effects of LDL transport through an artery by using a one-dimensional four-layer model, comparing it with a Newtonian fluid based on a viscosity value of 1.39 mPa s. They concluded that non-Newtonian effects through the wall should not be neglected when compared with a Newtonian fluid with this viscosity value, because the filtration velocity is influenced by non-Newtonian effects. More recently, Deyranlou et al. (2015) analyzed fluid–structure interactions for LDL accumulation by using a Carreau fluid model, coupled with a power-law porous media model. They also reported that, for large arteries, Newtonian model seems to be quite accurate in the lumen, while across the wall, it underestimates mass transport. However, an exhaustive analysis of concentration profiles is not present in their paper.

In the present study, a comprehensive investigation of non-Newtonian effects on LDL mass transport through an artery is presented. Three different non-Newtonian fluid models are used for the lumen, while a power-law fluid is used for the porous arterial wall. Detailed comparisons are presented for medium and large arteries. Non-Newtonian effects are also presented for the aorta–iliac bifurcation. It is established that while the rheological behavior of blood through arteries is non-Newtonian, a Newtonian fluid model can be employed for cases such as medium and large arteries.

2. Arterial wall modeling

2.1. Artery geometry

A sketch of an arterial wall is shown in Fig. 1a. The blood passes through the lumen. From the lumen, it tends to infiltrate through the arterial wall, carrying solutes like Low-Density Lipoprotein (LDL). The first layer that faces the free flow lumen is the endothelium, that is very important for fluid and solute filtration. After the endothelium, there is the tunica intima, which is made of connective tissue. The tunica intima is the layer in which an atherosclerotic plaque tends to grow. A thin layer of elastic tissue, namely the Internal Elastic Lamina (IEL), separates the tunica intima from the tunica media, that is composed of Smooth Muscle Cells (SMC) and connective tissues. After the tunica media, there is the tunica adventitia, which can be replaced by a proper boundary condition, as established in Yang and Vafai (2006). Geometrical parameters are in general taken after Chung and Vafai (2014), Iasiello et al. (2015) and Wang and Vafai (2015). The artery is 124 mm long and the lumen radius r_{lumen} is set equal to 3.1 mm. Along the wall, the thickness for the endothelium is 2 μm, 10 μm for the intima, 2 μm for the IEL, and 200 μm for the tunica media.

2.2. Mathematical model

2.2.1. Lumen region

The governing equations for the fluid flow are the steady-state Navier–Stokes equations for an incompressible flow without buoyancy effects:

$$\nabla \cdot \vec{V} = 0 \tag{1}$$

$$\rho \vec{V} \cdot \nabla \vec{V} = -\nabla p - \nabla \cdot \overline{\overline{\tau}} \tag{2}$$

with $\vec{V}$ the velocity, ρ blood density, p hydraulic pressure and $\overline{\overline{\tau}}$ is the stress tensor. In order to characterize the stress tensor $\overline{\overline{\tau}}$,

viscosity μ needs to be known. It can be modeled by means of different models:

- Newtonian fluid model, in which $\mu = 3.7$ mPa s (Chung and Vafai, 2014),
- Power-law fluid model, in which $\mu = \mu^*(\dot{\gamma})^{n-1}$, in which $\mu^* = 9.267$ mPa s^n and $n = 0.828$ (Kim et al., 2000)
- Carreau fluid model, in which $\mu = \mu_\infty + (\mu_z - \mu_\infty)\left[1+(\lambda\dot{\gamma})^2\right]^{\frac{n-1}{2}}$, in which $\mu_\infty = 3.45$ mPa s, $\mu_z = 56$ mPa s, $\lambda = 3.313$ s and $n = 0.3568$ (Cho and Kensey, 1991; Johnston et al., 2004)
- Carreau–Yasuda fluid model, in which $\mu = \mu_\infty + (\mu_z - \mu_\infty)\left[1+(\lambda\dot{\gamma})^q\right]^{\frac{n-1}{q}}$, in which $\mu_\infty = 3.45$ mPa s, $\mu_z = 56$ mPa s, $\lambda = 1.902$ s, $q = 1.25$ and $n = 0.22$ (Cho and Kensey, 1991).

The LDL mass transport can be represented by the following equation:

$$\vec{V} \cdot \nabla c = D\nabla^2 c \tag{3}$$

where c is the concentration and D is the diffusivity of blood through the lumen.

2.3. Arterial wall

For the arterial wall, a Newtonian fluid model with $\mu = 0.72$ mPa s is compared with a power-law non-Newtonian fluid. Governing equations for mass and momentum through the arterial wall can be presented in a general form (Yang and Vafai, 2006; Ai and Vafai, 2006; Khakpour and Vafai, 2008a; Chung and Vafai, 2012; Wang and Vafai, 2013, 2015; Kenjereš and de Loor, 2014; Iasiello et al., 2015):

$$\nabla \cdot \left\langle \vec{V} \right\rangle = 0 \tag{4}$$

$$\frac{\rho}{\varepsilon^2}\nabla \cdot \left(\left\langle \vec{V} \right\rangle \left\langle \vec{V} \right\rangle\right) = \rho \vec{g} - \nabla\langle p\rangle + \frac{\mu^*}{\varepsilon^n}\nabla\left\{\left|\sqrt{(1/2)(\langle\dot{\gamma}\rangle : \langle\dot{\gamma}\rangle)}\right|^{n-1}\langle\dot{\gamma}\rangle\right\} - \left(\frac{\mu^*\left|\left\langle \vec{V} \right\rangle\right|^{n-1}}{K^*} + \frac{C\rho\left\langle \vec{V} \right\rangle}{K^{1/2}}\right)\left\langle \vec{V} \right\rangle \tag{5}$$

In these equations, $\langle\rangle$ refers to the volume-averaged form of a variable, ε the porosity, $\vec{g}$ gravitational acceleration, p the pressure, μ^* the fluid viscosity of the non-Newtonian power-law fluid, n the power law fluid index, $\dot{\gamma}$ the local shear stress rate, K^* the power-law fluid permeability, K the permeability and C is the form coefficient. Based on physiological data, the inertial forces, buoyancy, viscous effects and microscopically inertial effects are negligible, as demonstrated in earlier literature (Yang and Vafai, 2006, 2008; Khakpour and Vafai, 2008a; Wang and Vafai, 2013). For the non-Newtonian fluid case, the comparison with experimental data that is reported in the next paragraph will demonstrate the reliability of the aforementioned assumptions.

The power-law Darcy equation for a porous medium can be written as:

$$\nabla\langle p\rangle = -\left(\frac{\mu^*\left|\left\langle \vec{V} \right\rangle\right|^{n-1}}{K^*}\right)\left\langle \vec{V} \right\rangle \tag{6}$$

The consistency index can be calculated from the following relationship:

$$\mu^* = \frac{\mu}{\dot{\gamma}^{n-1}} \tag{7}$$

where μ is the effective viscosity.

The power law permeability is defined by (Hayes et al., 1996):

$$K^* = \frac{1}{2\chi}\left(\frac{n\varepsilon}{3n+1}\right)^n\left(\frac{50K}{3\varepsilon}\right)^{\frac{(n+1)}{2}} \tag{8}$$

where the tortuosity factor χ is set equal to 25/12 (Christopher and Middleman, 1965).

Experimental data that describe viscosity as a function of shear stresses, from Graf and Barras (1979), are used in order to obtain the consistency index μ^* and the power law fluid index n that are going to be employed in the Darcy equation. Indeed, they reported viscosity as a function of shear stress. By performing a regression analysis, it is shown that a power-law function fits experimental data when $\mu^* = 3.16$ mPa s^n and $n = 0.81$.

Species concentration is calculated with the following stationary diffusion-convection-reaction equation that takes into account Staverman–Kedem–Katchalsky membrane transport equation:

$$(1-\sigma)\left\langle \vec{V} \right\rangle \cdot \nabla\langle c\rangle = D_{eff}\nabla^2\langle c\rangle - k\langle c\rangle \tag{9}$$

where σ is the Staverman reflection coefficient, D_{eff} the effective diffusivity and k the reaction term, that takes into account the uptake of LDL that occurs in the tunica media (Chung and Vafai, 2014). This reaction term is zero in the layers that are not the tunica media.

2.4. Boundary conditions and numerical modeling

A 2D axisymmetrical model has been used for computations. With references to Fig. 1a, the symmetry axis is the axis of the lumen, with its origin located at the beginning of the artery. The axial and radial coordinates are referred with the letters z and r, respectively. The well-established boundary conditions used here are in general taken after Chung and Vafai (2014), Wang and Vafai (2015) and Iasiello et al. (2015). A parabolic and fully developed flow is prescribed at the inlet section of the lumen in Fig. 1a:

$$u = 2u_m\left(1-(r/r_{lumen})\right)^2 \tag{10}$$

where u is the axial component of velocity, u_m the mean velocity, namely 0.169 m/s (Yang and Vafai, 2006; Wang and Vafai, 2013; Chung and Vafai, 2014), r the radius and r_{lumen} the lumen radius, namely 3.1 mm, that is relative to a medium artery (Prosi et al., 2005). The concentration at the inlet section c_0 is taken as $28.6 \cdot 10^{-3}$ mol/m^3 (Chung and Vafai, 2014). Pressure is set as 100 mmHg at the lumen outlet, while it is 30 mmHg at the media/adventitia interface, causing a 70 mmHg intramural pressure (Yang and Vafai, 2006; Ai and Vafai 2006; Chung and Vafai, 2012, 2014). A sensitivity analysis performed by Yang and Vafai (2006) has shown that this is the most realistic boundary condition. All the other boundaries are modeled with a slip condition for the momentum equation, and with a zero normal diffusive flux for the concentration equation. Continuity conditions for momentum and mass transfer are invoked at the interior boundaries. For the mass transfer, Staverman filtration is also considered within the interface continuity condition:

$$\left[(1-\sigma)vc - D_{eff}\frac{\partial c}{\partial r}\right]\Big|_+ = \left[(1-\sigma)vc - D_{eff}\frac{\partial c}{\partial r}\right]\Big|_- \tag{11}$$

where v is the radial component of the velocity, namely the filtration velocity.

Thermophysical properties such as permeability K, diffusivities D and D_{eff}, and Staverman reflection coefficient σ, that close governing Eqs. (1)–(4), (6) and (9) are in general taken after Chung and Vafai (2014) and Iasiello et al. (2015). Blood density has been set equal to 1070 kg/m^3 (Chung and Vafai, 2012), while the fraction and the half-width of leaky junctions values are set as $5 \cdot 10^{-4}$ and

14.343 nm, respectively (Chung and Vafai, 2012). Governing equations with the boundary conditions previously described are solved with a finite-element scheme by using the commercial code COMSOL Multiphysics. A rectangular mapped mesh of about of 500,000 elements has been built, and its independence has been checked. Mass balances have been verified, while a 10^{-6} RMS convergence criterion has been used.

3. Results

3.1. Arterial wall

Filtration velocities along the lumen/endothelium interface are reported for both Newtonian and non-Newtonian power-law fluid as a function of the axial coordinate in Fig. 2a, for intramural

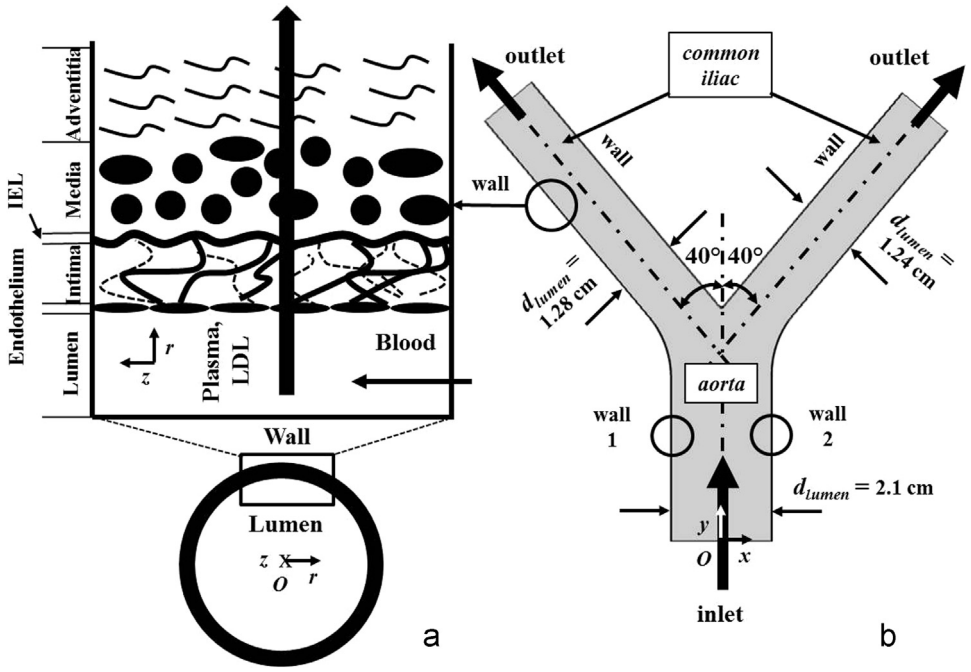

Fig. 1. Schematic of (a) an arterial wall and (b) aorta–common iliac bifurcation.

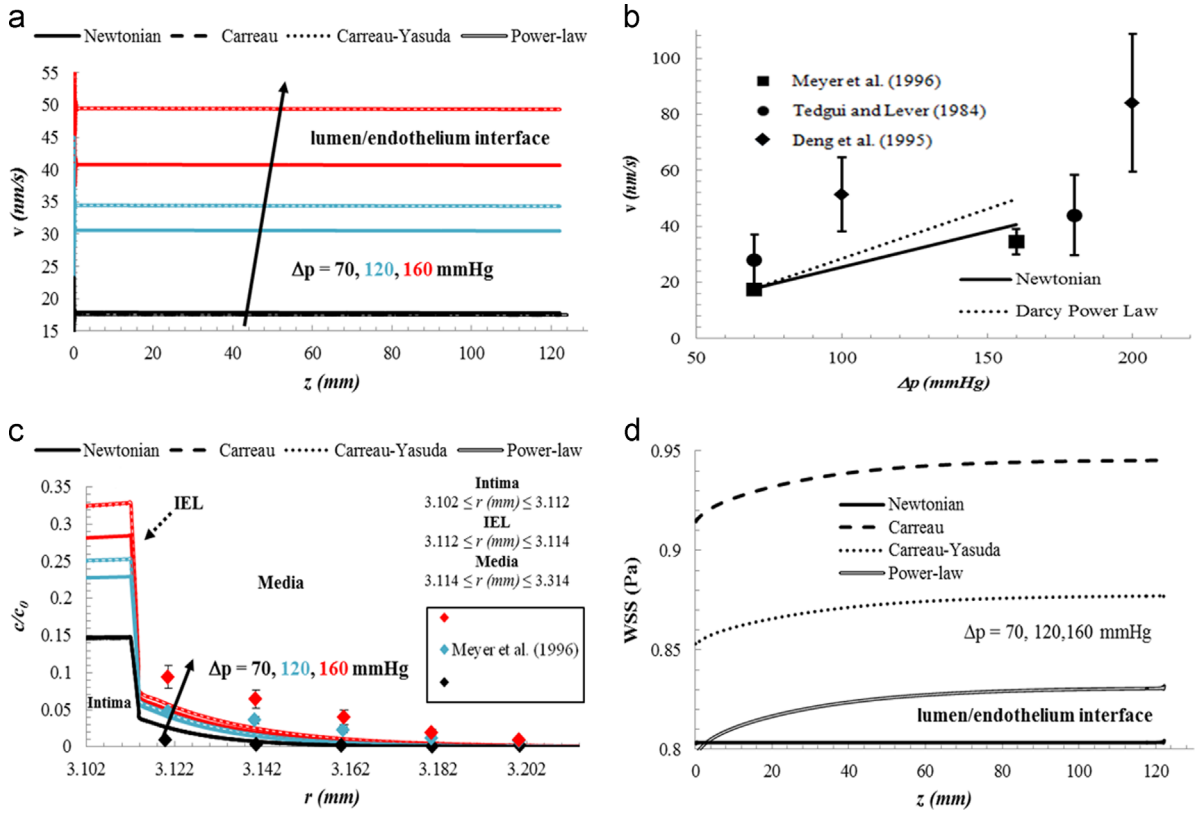

Fig. 2. (a) Filtration velocities for different rheological models under hypertensive conditions, (b) comparisons with experimental results, (c) concentration profiles along the arterial wall for different rheological models under hypertensive conditions, and (d) WSS along the lumen/endothelium interface.

pressure values of $\Delta p = 70$, 120 and 160 mmHg. Differences between such curves are negligible for a healthy case, while they increase with intramural pressure, reaching about 15% for the highest intramural pressure case.

A comparison with experimental results from literature is reported in Fig. 2b. Such experimental results are relative to experiments carried out on animals. Meyer et al. (1996) found that that filtration velocity for the aorta of a rabbit is 17.5 ± 0.15 nm/s when $\Delta p = 70$ mmHg, while Tedgui and Lever (1984) reported a value of 28.0 ± 0.91 nm/s. Hypertensive case was also considered by Meyer et al. (1996), obtaining a value of 34.5 ± 4.6 nm/s when $\Delta p = 160$ mmHg, while Tedgui and Lever (1984) have reported a value of 44.0 ± 14.4 nm/s when $\Delta p = 180$ mmHg, based on Deng et al. (1995), who carried out experiments on canine carotid arteries. From our results, it is possible to see that both Newtonian and power-law non-Newtonian models match pretty well with the experimental results.

In Fig. 2c, results for the arterial wall are reported in terms of concentration profiles, under hypertension conditions. It is shown that non-Newtonian effects on LDL deposition through the wall are negligible when a healthy case is considered, obtaining a difference of less than 1%, while such difference increases with hypertension, reaching about the 10% when $\Delta p = 160$ mmHg. These differences are in line with the differences in filtration velocities between non-Newtonian and Newtonian cases, that increase with intramural pressure. Comparisons with experimental results from Meyer et al. (1996) for the LDL concentration through the media layer of the rabbit aortic wall are also reported in Fig. 2c, for various intramural pressures. A good agreement has been found in the media layer for both Newtonian and non-Newtonian models. As can be seen the concentration profiles obtained with the Newtonian model are practically overlapped with those from Chung and Vafai (2012, 2014) and Iasiello et al. (2015), whose models were also validated.

3.2. Free flow

Results for the free flow of the lumen are shown here for Newtonian fluid and different non-Newtonian fluid models. WSS are calculated as the product of the dynamic viscosity and the shear rate. In Fig. 2d, WSS are reported for different rheological models. It is shown that there is a slight increase along the axial coordinate, due to the non-Newtonian nature of the fluid. The largest difference was found between the Newtonian and the Carreau fluid model. The Carreau–Yasuda fluid model provides little difference, while with a power-law fluid model the WSS are very close to the Newtonian fluid case. Concentration accumulation along the lumen/endothelium interface is reported in Fig. 3. Qualitative trends of the curves are the same for the all rheological models that have been used. Differences are negligible for all the investigated intramural pressure values. The maximum difference that has been found is about 2%, relative to the $\Delta p = 160$ mmHg case.

3.3. Artery size effect

It is widely known that arteries can be classified in terms of their size. Starting from a lumen radius of 3.1 mm, that is typical of a medium artery, simulations are carried out by varying this radius, in order to analyze non-Newtonian effects also when a large artery is considered. Computations are performed at equal inlet velocities. Intramural pressure is set as 70 mmHg. Results for the WSS and for the concentration polarization are shown in Figs. 4 and 5. It is shown that, in general, the WSS reduce when artery dimensions increase, while the differences between non-Newtonian and Newtonian fluid models remain almost the same as the case studied in Fig. 2d. For the concentration accumulation

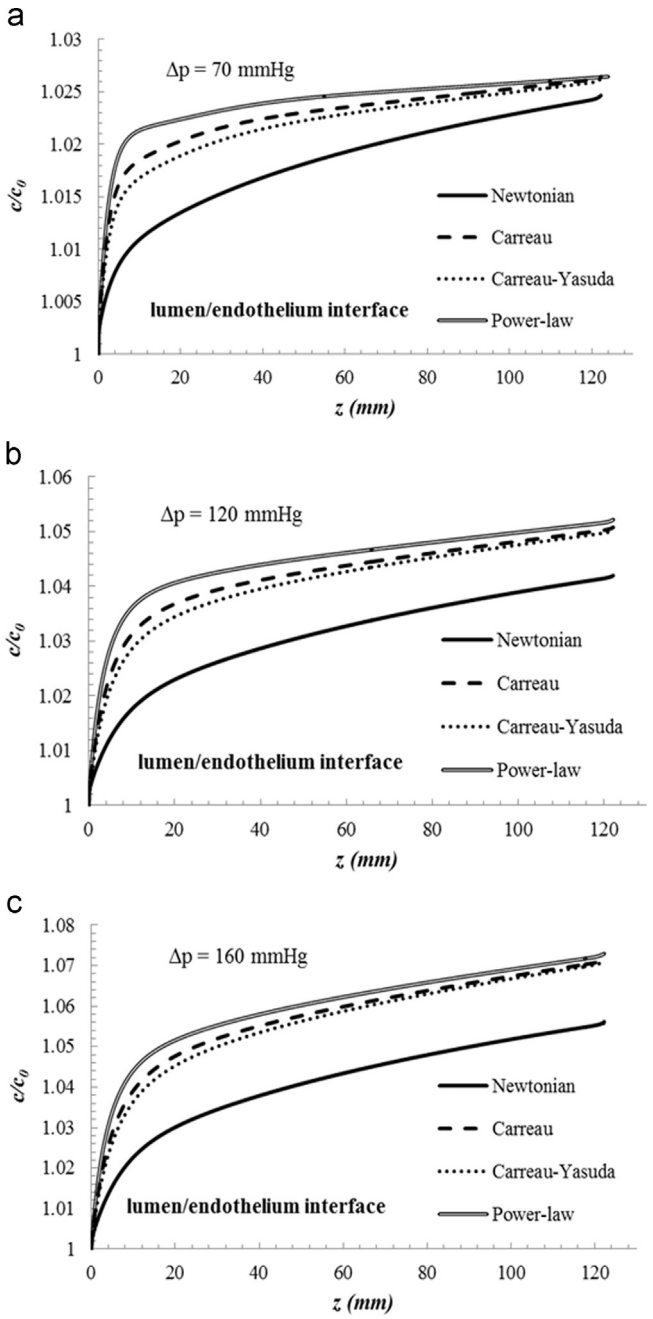

Fig. 3. LDL concentration accumulation along the lumen/endothelium interface for different rheological models with (a) $\Delta p = 70$ mmHg, (b) $\Delta p = 120$ mmHg and (c) $\Delta p = 160$ mmHg.

along the lumen/endothelium interface reported in Fig. 5, it is shown that it increases with the diameter. The reason for this is that for larger diameters more solvent tends to penetrate the arterial wall, causing an increase of concentration through the lumen. Again, non-Newtonian flow models seem to provide similar values of concentration. Differences of not more than 2% where found.

For the arterial wall, it has been found that differences in filtration velocity and concentration profiles are negligible. Differences of less than 0.1% can be pointed out because of the differences in concentration polarization along the lumen/endothelium interface.

The maximum percentage differences that have been found between Newtonian and non-Newtonian model with reference to

the concentration polarization along the lumen/endothelium interface are shown in Fig. 5d, for different arteries sizes and intramural pressures. It can be seen that differences relative to the maximum value are quite small for the concentration polarization along the lumen/endothelium interface. As such both Newtonian and non-Newtonian models can be used in modeling LDL mass transport in a medium or large artery.

4. The aorta–iliac bifurcation

Non-Newtonian effects can arise in particular when geometries become more complex (Cho and Kensey, 1991; Lou and Yang (1993); Mandal, 2005). In this work, the aorta–iliac bifurcation is analyzed with the comprehensive multilayer model. The geometry of the bifurcation is presented in Fig. 1b. Geometrical parameters are taken from Shah et al. (1978). Both internal and external iliac angles are considered to be 40°, that is the most symmetric case (Shah et al., 1978; Khakpour and Vafai, 2008b). The lumen diameter d_{lumen} for the right common iliac, wall 1, is 1.28 cm, with a length of 6.10 cm. For the left common iliac, wall 2, $d_{lumen}=1.24$ cm and the length is 5.80 cm. The diameter of the aorta is $d_{lumen}=2.10$ cm, with a length of 5.00 cm. The left and right common iliac diameters are different, causing a non-perfect symmetry. Governing equations, boundary conditions and transport coefficients are the same as those that have been used for the straight artery. Due to the more complex geometry, a triangular mesh with boundary layer has been used. Grid independence has been verified by checking the dimensionless LDL concentration c/c_0 profiles along the lumen/endothelium interface, by systematically increasing the number of elements.

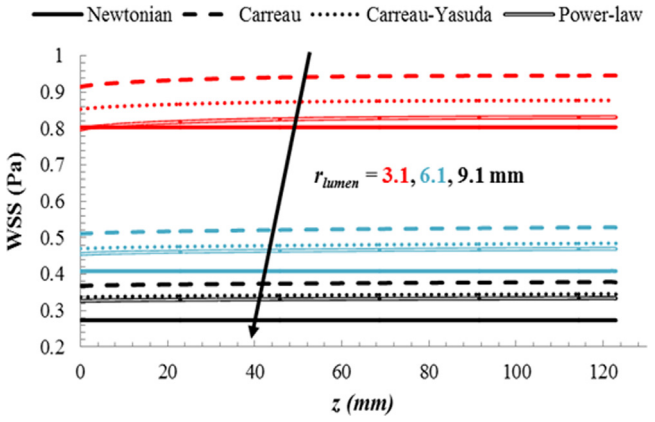

Fig. 4. WSS along the lumen/endothelium interface for different rheological models for different arteries sizes.

Non-Newtonian effects are analyzed by varying the Reynolds number $Re=2\rho u_m r_{lumen}/\mu$ by means of the mean inlet velocity u_m. Reynolds number effects on WSS and on lumen/endothelium LDL accumulation are shown in Fig. 6, for a Newtonian fluid. The number 1 designation is relative to the side in which the diameter of the iliac becomes the highest, while the number 2 designation is relative to the other case. In general, it is shown that WSS increase with Reynolds number, while concentration accumulation increases with lower Reynolds number.

In Fig. 6a it is shown that WSS remain constant just before the curve. A rapid increase occurs when the curve starts, followed by a very fast decrease of the stresses. With higher Reynolds number, flow separation may occur due to the inversion of the WSS. The concentration accumulation is reported in Fig. 6b. Concentration

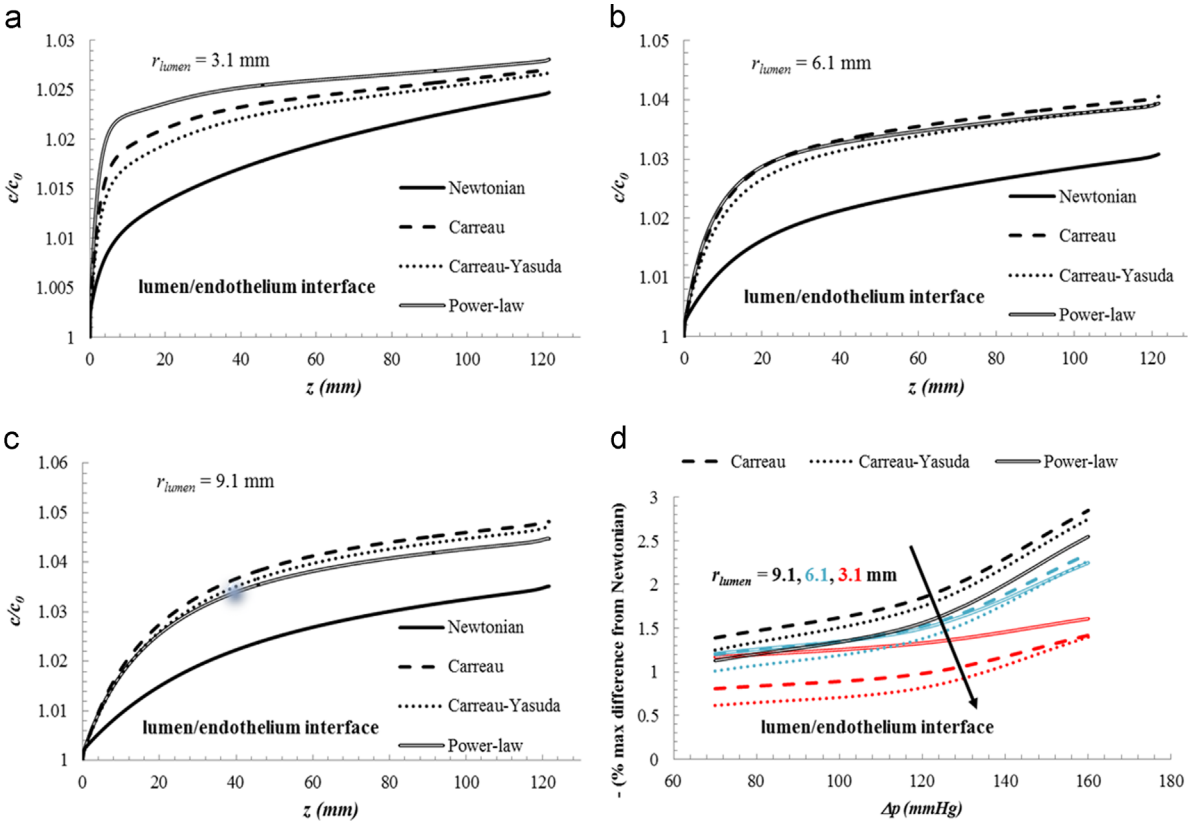

Fig. 5. LDL concentration accumulation along the lumen/endothelium interface for different rheological models with (a) $r_{lumen}=3.1$ mm, (b) $r_{lumen}=6.1$ mm and (c) $r_{lumen}=9.1$ mm, and (d) maximum percentage differences between Newtonian model and other rheological models for the concentration along the lumen/endothelium interface.

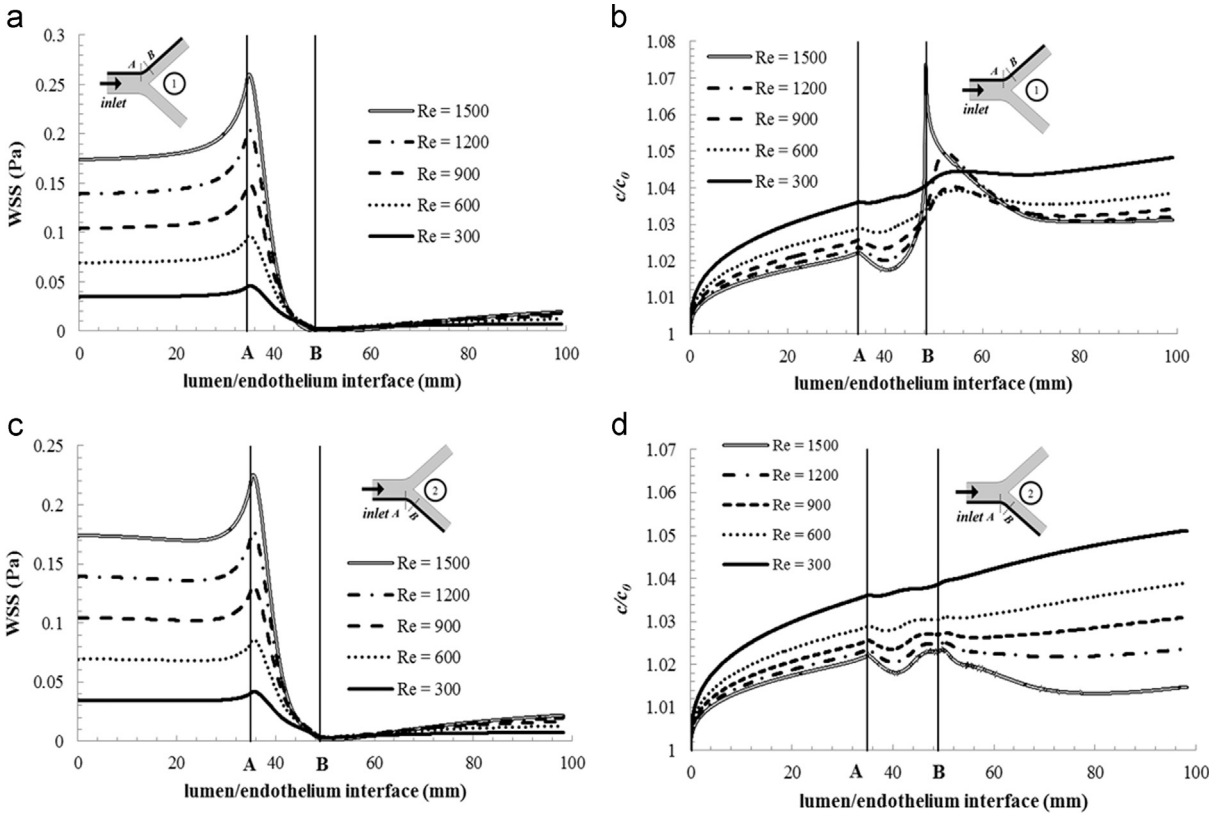

Fig. 6. WSS and LDL concentration accumulation for the Newtonian model and with different Reynolds numbers: (a) and (b) are relative to upper wall 1, while (c) and (d) refer to lower wall 2.

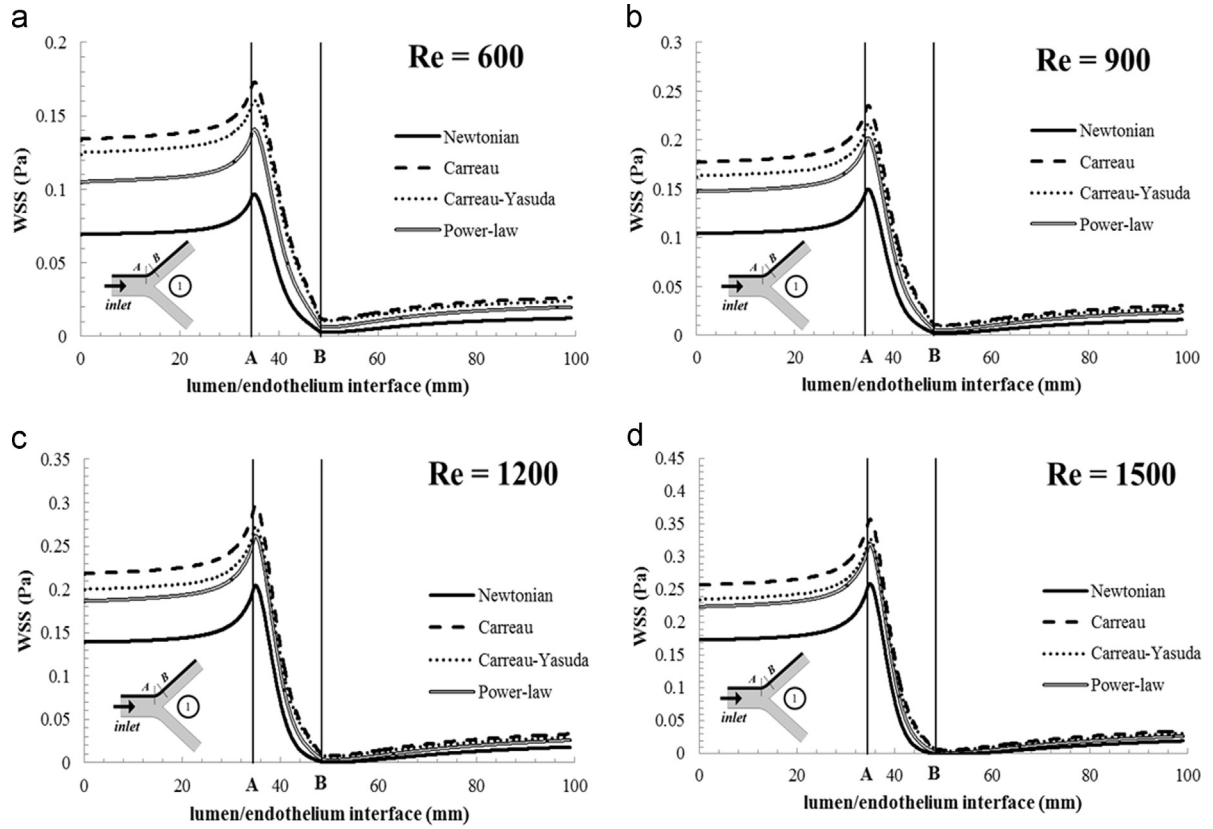

Fig. 7. Reynolds number effects on WSS along the lumen/endothelium interface for different rheological models: upper wall 1.

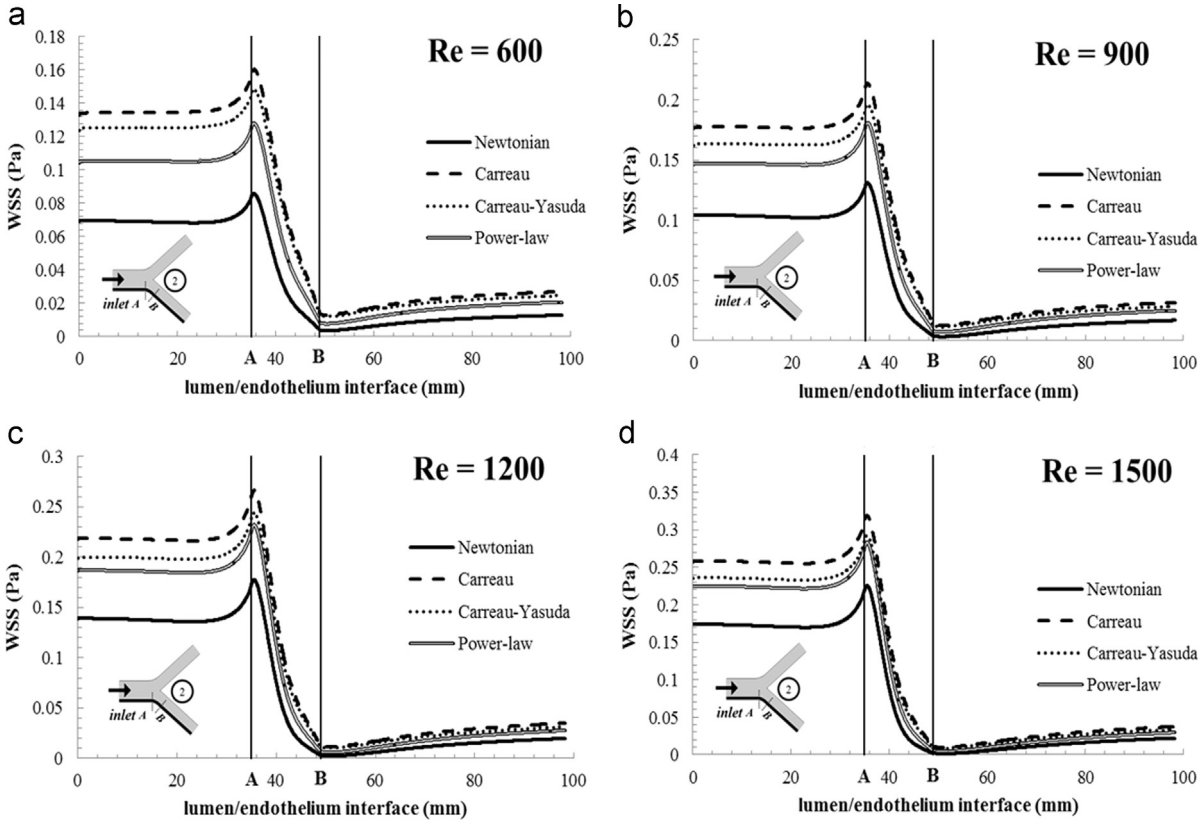

Fig. 8. Reynolds number effects on WSS along the lumen/endothelium interface for different rheological models: lower wall 2.

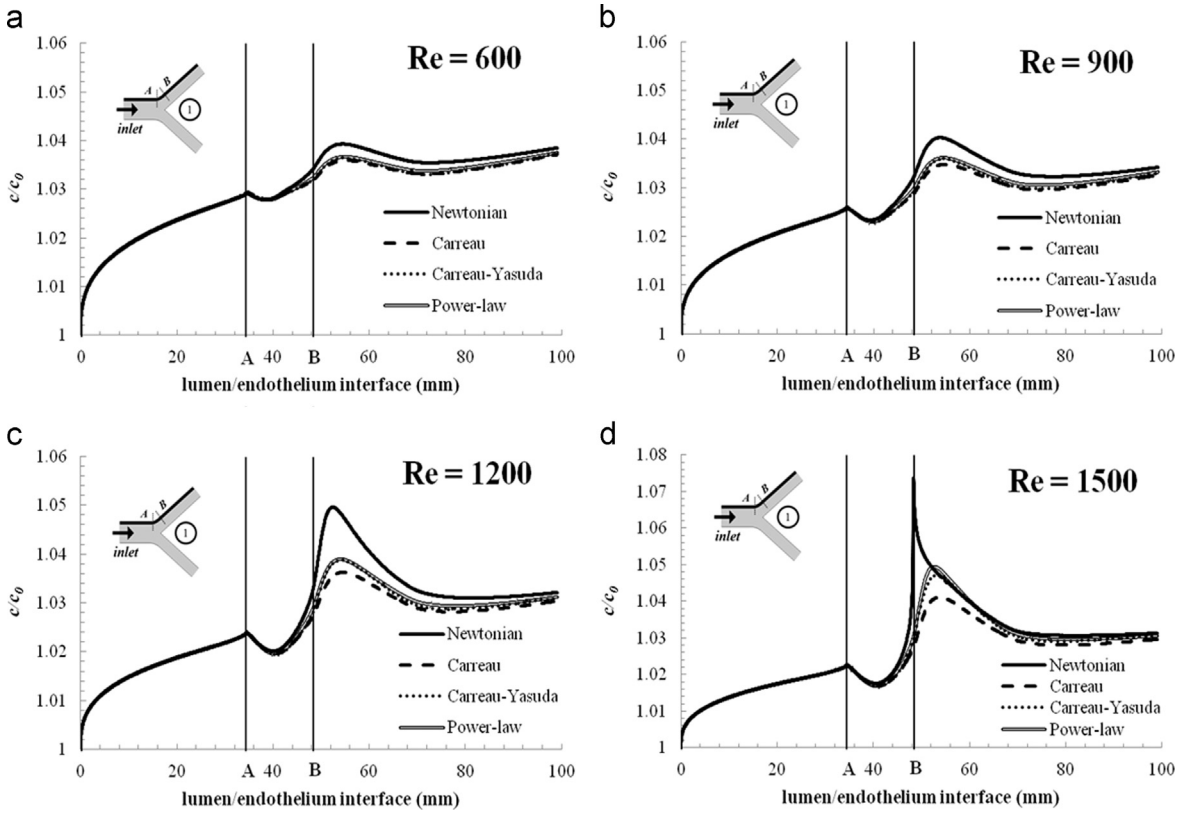

Fig. 9. Reynolds number effects on LDL concentration accumulation along the lumen/endothelium interface for different rheological models: upper wall 1.

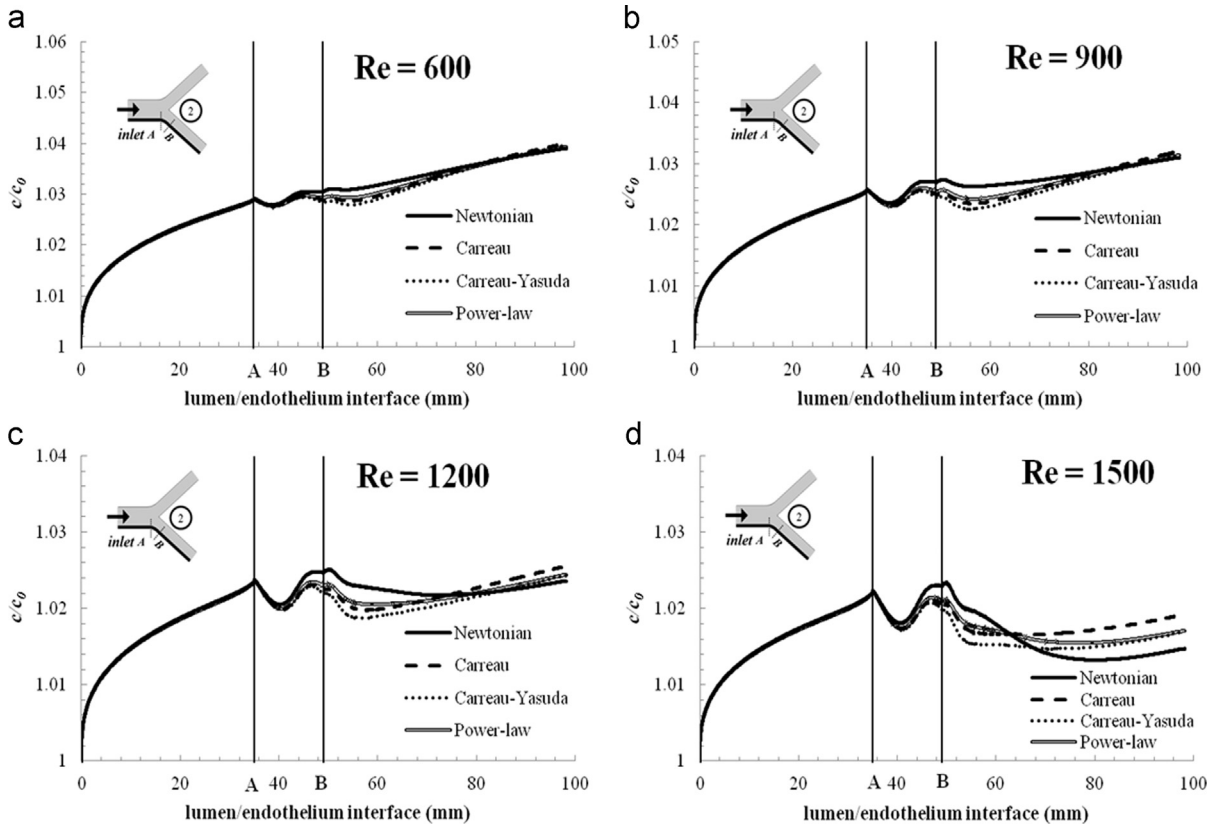

Fig. 10. Reynolds number effects on LDL concentration accumulation along the lumen/endothelium interface for different rheological models: lower wall 2.

increases along the straight part of the aorta due to the polarization, decreasing a little bit in the same zone in which WSS increase, then re-increasing in the straight iliac. At higher Reynolds number, concentration profiles become altered due to the flow recirculation. At $Re=1500$, it is possible to see a strong peak, due to a very enhanced recirculation.

In Fig. 6c and d, WSS and concentration are reported for the other iliac, namely the one that has a smaller diameter. It seems that recirculation does not occur. However, after the curvature, it seems that concentration is not rapidly increasing when Reynolds number is high. For $Re=1500$, concentration starts to increase only around the exit section. This is because the bifurcation is not symmetric.

In Figs. 7–10, non-Newtonian effects on the aorta–iliac bifurcation are analyzed. For the WSS depicted in Figs. 7 and 8, trends are similar for all the non-Newtonian models. The Carreau model provides the highest values and difference compared to a Newtonian fluid, while the Carreau–Yasuda and power-law fluid provide the lowest differences. Considering only the $Re=1200$ and 1500 cases reported in Figs. 7c and d and 8c and d, it is shown that flow separation does not occur when a non-Newtonian fluid model is employed. This means that more attention is needed when curves of particular geometries are modeled.

Concentration accumulation results are reported in Figs. 9 and 10. When Reynolds number is low or when recirculation does not occurs, it seems that there are no significant differences between various fluid models. Particular attention is needed for the cases in which recirculation may occur, at high Reynolds numbers. Such cases are depicted in Fig. 9c and d, for case 1. All the concentration profiles have higher gradients in the curvature zone, because of the deceleration of the fluid. Newtonian profiles seem to be more alterated, because it predicts flow separation, i.e. WSS has a negative sign. At $Re=1500$, this phenomena is a bit more enhanced, causing a more pronounced peak for the Newtonian case, compared with the other fluid models, with more regular profiles. This means that, as previously argued for the WSS, the non-Newtonian fluid model in curvatures and recirculation zones are a bit more pronounced.

5. Conclusions

A comprehensive analysis of non-Newtonian fluid effects on LDL mass transport through an artery was presented in this work. The free flow through the lumen has been modeled with three different non-Newtonian fluid models, while the arterial wall has been predicted by means of a power-law fluid model for a porous medium. Our results show that the non-Newtonian effects on mass transport are negligible for a normal intramural pressure. For hypertensive cases, these differences are still relatively negligible on the lumen/endothelium interface, reaching a difference of mainly less than 10% through the wall, that can be still considered as negligible. Non-Newtonian effects remain still negligible when larger arteries are considered. Finally, non-Newtonian effects on mass transport for an aorta–iliac bifurcation were analyzed. It has been shown that such differences are also negligible at low Reynolds numbers. At higher Reynolds numbers, because flow recirculation may occur, a non-Newtonian fluid model might be a little more accurate in predicting LDL concentration profiles.

Conflict of interest

There is no conflict of interest. This manuscript has not been submitted to anywhere else.

Acknowledgments

The stay of Marcello Iasiello at the University of California, Riverside was financially supported by UniNA and Compagnia di San Paolo, in the frame of Program STAR.

References

Ai, L., Vafai, K., 2006. A coupling model for macromolecule transport in a stenosed arterial wall. Int. J. Heat Mass Transf. 49, 1568–1591.
Cho, Y.I., Kensey, K.R., 1991. Effects of the non-Newtonian viscosity of blood on flows in a diseased arterial vessel. Part 1: steady flows. Biorheology 28, 241–262.
Christopher, R.H., Middleman, S., 1965. Power-law flow through a packed tube. Ind. Eng. Chem. Fundam. 4, 422–426.
Chung, S., Vafai, K., 2012. Effect of the fluid–structure interactions on low-density lipoprotein transport within a multi-layered arterial wall. J. Biomech. 45, 371–381.
Chung, S., Vafai, K., 2013. Low-density lipoprotein transport within a multi-layered arterial wall – effect of the atherosclerotic plaque/stenosis. J. Biomech. 46, 574–585.
Chung, S., Vafai, K., 2014. Mechanobiology of low-density lipoprotein transport within an arterial wall – impact of hyperthermia and coupling effects. J. Biomech. 47, 137–147.
Deng, X., Marois, Y., How, T., Merhi, Y., King, M., Guidoin, R., Karino, T., 1995. Luminal surface concentration of lipoprotein (LDL) and its effect on the wall uptake of cholesterol by canine carotid arteries. J. Vasc. Surg. 21, 135–145.
Deyranlou, A., Niazmand, H., Sadeghi, M.-R., 2015. Low-density lipoprotein accumulation within a carotid artery with multilayer elastic porous wall: fluid–structure interaction and non-Newtonian considerations. J. Biomech. 48, 2948–2959.
Fazli, S., Shirani, E., Sadeghi, M.R., 2011. Numerical simulation of LDL mass transfer in a common carotid artery under pulsatile flows. J. Biomech. 44, 68–76.
Graf, C., Barras, J.P., 1979. Rheological properties of human blood plasma—a comparison of measurements with three different viscometers. Experientia 35, 224–225.
Hayes, R.E., Afacan, A., Boulanger, B., Shenoy, A.V., 1996. Modelling the flow of power law fluids in a packed bed using a volume-averaged equation of motion. Transp. Porous Media 23, 175–196.
Hong, J., Fu, C., Lin, H., Tan, W., 2012. Non-Newtonian effects on low-density lipoprotein transport in the arterial wall. J. Non-Newton. Fluid Mech. 189, 1–7.
Huang, Y., Rumschitzki, D., Chien, S., Weinbaum, S., 1997. A fiber matrix model for the filtration through fenestral pores in a compressible arterial intima. Am. J. Physiol. 272, H2023–H2039.
Iasiello, M., Vafai, K., Andreozzi, A., Bianco, N., Tavakkoli, F., 2015. Effects of external and internal hyperthermia on LDL transport and accumulation within an arterial wall in the presence of a stenosis. Ann. Biomed. Eng. 43, 1585–1599.
Johnston, B.M., Johnston, P.R., Corney, S., Kilpatrick, D., 2004. Non-Newtonian blood flow in human right coronary arteries: steady state simulations. J. Biomech. 37, 709–720.
Johnston, B.M., Johnston, P.R., Corney, S., Kilpatrick, D., 2006. Non-Newtonian blood flow in human right coronary arteries: transient simulations. J. Biomech. 39, 1116–1128.
Keller, B., Clubb Jr., F., Dubini, G., 2011. A review of atherosclerosis and mathematical transport models. In: IFMBE Proceedings. Volume 36. Springer Berlin Heidelberg, Berlin.
Kenjereš, S., de Loor, A., 2014. Modelling and simulation of low-density lipoprotein transport through multi-layered wall of an anatomically realistic carotid artery bifurcation. J. R. Soc. Interface 11, 20130941.
Khakpour, M., Vafai, K., 2008a. A comprehensive analytical solution of macromolecular transport within an artery. Int. J. Heat Mass Transf. 51, 2905–2913.
Khakpour, M., Vafai, K., 2008b. Effects of gender-related geometrical characteristics of aorta–iliac bifurcation on hemodynamics and macromolecule concentration distribution. Int. J. Heat Mass Transf. 51, 5542–5551.
Kim, S., Cho, Y.I., Jeon, A.H., Hogenauer, B., Kensey, K.R., 2000. A new method for blood viscosity measurement. J. Non-Newton. Fluid Mech. 94, 47–56.
Lantz, J., Karlsson, M., 2012. Large eddy simulation of LDL surface concentration in a subject specific human aorta. J. Biomech. 45, 537–542.
Lou, Z., Yang, W.J., 1993. A computer simulation of the non-Newtonian blood flow at the aortic bifurcation. J. Biomech. 26, 37–49.
Liu, X., Fan., Y., Deng, X., Zhan, F., 2011. Effect of non-Newtonian and pulsatile blood flow on mass transport in the human aorta. J. Biomech. 44, 1123–1131.
Mandal, P.K., 2005. An unsteady analysis of non-Newtonian blood flow through tapered arteries with a stenosis. Int. J. Non-Linear Mech. 40, 151–164.
Meyer, G., Merval, R., Tedgui, A., 1996. Effects of pressure-induced stretch and convection on low-density lipoprotein and albumin uptake in the rabbit aortic wall. Circ. Res. 79, 532–540.
Nematollahi, A., Shirani, E., Sadeghi, M.R., Mirzaee, I., 2015. Effects of shear-dependent transport properties on lumen surface concentration of LDL particles in stenosed carotid artery. Meccanica 50, 1–14.
Perktold, K., Karner, G., Leuprecht, A., Hofer, M., 1999. Influence of non-Newtonian flow behavior on local hemodynamics. ZAMM 79, 187–190.
Prosi, M., Zunino, P., Perktold, K., Quarteroni, A., 2005. Mathematical and numerical models for transfer of low-density lipoproteins through the arterial walls: a new methodology for the model set up with applications to the study of disturbed lumenal flow. J. Biomech. 38, 903–917.
Razavi, A., Shirani, E., Sadeghi, M.R., 2011. Numerical simulation of blood pulsatile flow in a stenosed carotid artery using different rheological models. J. Biomech. 44, 2021–2030.
Ross Ethier, C., Simmons, C.A., 2007. Introductory Biomechanics: From Cells to Organisms. Cambridge University Press, New York City, pp. 119–163.
Shah, P.M., Scarton, H.A., Tsapogas, M.J., 1978. Geometric anatomy of the aortic–common iliac bifurcation. J. Anat. 126, 451–458.
Sun, B., Vallez, L.J., Plourde, B.D., Stark, J.R., Abraham, J.P., 2015. Influence of supporting tissue on the deformation and compliance of healthy and diseased arteries. J. Biomed. Sci. Eng. 8, 490–499.
Tada, S., Tarbell, J.M., 2000. Interstitial flow through the internal elastic lamina affects shear stress on arterial smooth muscle cells. Am. J. Physiol. Heart Circ. Physiol. 278, H1589–H1597.
Taylor, F., Huffman, M.D., Macedo, A.F., Moore, T.H., Burke, M., Davey Smith, G., Ward, K., Ebrahim, S., 2013. Statins for the primary prevention of cardiovascular disease. Cochrane Database Syst. Rev. 1, CD004816.
Tedgui, A., Lever, M.J., 1984. Filtration through damaged and undamaged rabbit thoracic aorta. Am. J. Physiol. Heart Circ. Physiol. 247, H784–H791.
Vallez, L.J., Sun, B., Plourde, B.D., Abraham, J.P., Staniloe, C.S., 2015. Numerical analysis of arterial plaque thickness and its impact on artery wall compliance. J. Cardiovasc. Med. Cardiol. 2, 26–34.
Wang, S., Vafai, K., 2013. Analysis of the effect of stent emplacement on LDL transport within an artery. Int. J. Heat Mass Transf. 64, 1031–1040.
Wang, S., Vafai, K., 2015. Analysis of low-density lipoprotein (LDL) transport within a curved artery. Ann. Biomed. Eng. 43, 1571–1584.
Yang, N., Vafai, K., 2006. Modeling of low-density lipoprotein (LDL) transport in the artery – effects of hypertension. Int. J. Heat Mass Transf. 49, 850–867.
Yang, N., Vafai, K., 2008. Low-density lipoprotein (LDL) transport in an artery – a simplified analytical solution. Int. J. Heat Mass Tran. 51, 497–505.
Yilmaz, F., Gündoğdu, M.Y., 2008. A critical review on blood flow in large arteries; relevance to blood rheology, viscosity models, and physiologic conditions. Korea-Aust. Rheol. J. 20, 197–211.